

## Evidences of landslide earthquake triggering due to self-excitation process

F. Bozzano · L. Lenti · Salvatore Martino ·  
A. Paciello · G. Scarascia Mugnozza

Received: 20 March 2009 / Accepted: 29 December 2009 / Published online: 2 February 2010  
© Springer-Verlag 2010

**Abstract** The basin-like setting of stiff bedrock combined with pre-existing landslide masses can contribute to seismic amplifications in a wide frequency range (0–10 Hz) and induce a self-excitation process responsible for earthquake-triggered landsliding. Here, the self-excitation process is proposed to justify the far-field seismic trigger of the Cerda landslide (Sicily, Italy) which was reactivated by the 6th September 2002 Palermo earthquake ( $M_s = 5.4$ ), about 50 km far from the epicentre. The landslide caused damage to farm houses, roads and aqueducts, close to the village of Cerda, and involved about  $40 \times 10^6 \text{ m}^3$  of clay shales; the first ground cracks due to the landslide movement formed about 30 min after the main shock. A stress–strain dynamic numerical modelling, performed by FDM code FLAC 5.0, supports the notion that the combination of local geological setting and earthquake frequency content played a fundamental role in the landslide reactivation. Since accelerometric records of the triggering event are not available, dynamic equivalent inputs have been used for the numerical

modelling. These inputs can be regarded as representative for the local ground shaking, having a PGA value up to  $0.2 \text{ m/s}^2$ , which is the maximum expected in 475 years, according to the Italian seismic hazard maps. A 2D numerical modelling of the seismic wave propagation in the Cerda landslide area was also performed; it pointed out amplification effects due to both the structural setting of the stiff bedrock (at about 1 Hz) and the pre-existing landslide mass (in the range 3–6 Hz). The frequency peaks of the resulting amplification functions ( $A(f)$ ) fit well the  $H/V$  spectral ratios from ambient noise and the  $H/H$  spectral ratios to a reference station from earthquake records, obtained by in situ velocimetric measurements. Moreover, the Fourier spectra of earthquake accelerometric records, whose source and magnitude are consistent with the triggering event, show a main peak at about 1 Hz. This frequency value well fits the one amplified by the geological setting of the bedrock in correspondence with the landslide area, which is constituted of marly limestones and characterised by a basin-like geometry.

**Keywords** Earthquake-triggered landslide · Local seismic response · Italy

---

F. Bozzano · S. Martino (✉) · G. Scarascia Mugnozza  
Department of Earth Sciences, Research Centre for Geological Risks (CERI–Valmontone), University of Rome “Sapienza”,  
P.le A.Moro 5, 00185 Rome, Italy  
e-mail: salvatore.martino@uniroma1.it

L. Lenti  
Laboratoire Central des Ponts et Chaussées (LCPC),  
Paris East University, 58 Boulevard Lefebvre,  
75732 Paris Cedex 15, France

A. Paciello  
Agenzia Nazionale per le Nuove Tecnologie,  
l’Energia e lo Sviluppo Economico Sostenibile ENEA–C.R.  
Casaccia, Via Anguillarese 301, S.Maria di Galeria,  
00123 Roma, Italy

### Introduction

Worldwide case histories demonstrate that earthquake-induced landslides affect both rock and soil slopes in different ways (Keefer 1984; Hutchinson 1987; Sassa 1996; Rodriguez et al. 1999; Luzi and Pergalani 2000; Prestininzi and Romeo 2000; Sassa et al. 2005; Lin et al. 2008; Towhata et al. 2008) and that these ground effects are often responsible for the greatest damages and losses due to earthquakes (Bird and Bommer 2004). Analyses performed according to the Newmark (1965) approach at

regional scale allow to develop different earthquake-triggered landslide scenarios (Faccioli 1995; Luzi and Pergalani 1996, 2000; Miles and Ho 1999; Romeo 2000; MahdaviFar et al. 2008).

Empirical correlations have been proposed (Keefer 1984; Sassa et al. 1996; Fukuoka et al. 1997; Rodriguez et al. 1999; Romeo 2000) between the epicentral distance of the landslides and the magnitude of the triggering earthquakes; as a result, for each type of landslide a maximum expected epicentral distance can be estimated with reference to the earthquake magnitude. Nevertheless, these relations may be altered by local site conditions (tectonic features, stratigraphic conditions, morphology), which amplify the seismic input (Gallipoli et al. 2000; Havenith et al. 2003a, b; Meric et al. 2005; Bordoni et al. 2006; Méric et al. 2007). The possible interactions between seismic input, slope and pre-existing landslide mass were recently analysed by Bozzano et al. (2008c) for the seismically induced Salcito landslide (Bozzano et al. 2004a, b). This landslide shows features very similar that at Cerda, since both of them occurred in far-field (i.e. about 50 km far from the earthquake epicentre), involved a volume of some tens of millions of cubic metres of clay shales and the related ground cracks formed some ten of minutes after the triggering seismic event (Bozzano et al. 2008b).

It was pointed out from both in situ velocimetric measurements (ambient noise and weak motion) and numerical models (Bozzano et al. 2008c) that the reactivation of the Salcito landslide can be strongly related to the low-frequency content of the triggering event as well as to the geological setting of the slope, since the pre-existing landslide mass is included within a basin-like system, responsible for local 2D seismic amplification effects, according to a geological setting characterised by a basin-

like geometry of the stiff bedrock (Bard and Bouchon 1985).

These findings are in agreement with some field experiments (Steimen et al. 2003; Roten et al. 2004; Lenti et al. 2009) showing that evidences of 2D amplification effects can be observed from ambient noise records as well as from records of low-moderate magnitude earthquakes, after removing the effects due to source and wave propagation (Borcherdt 1994).

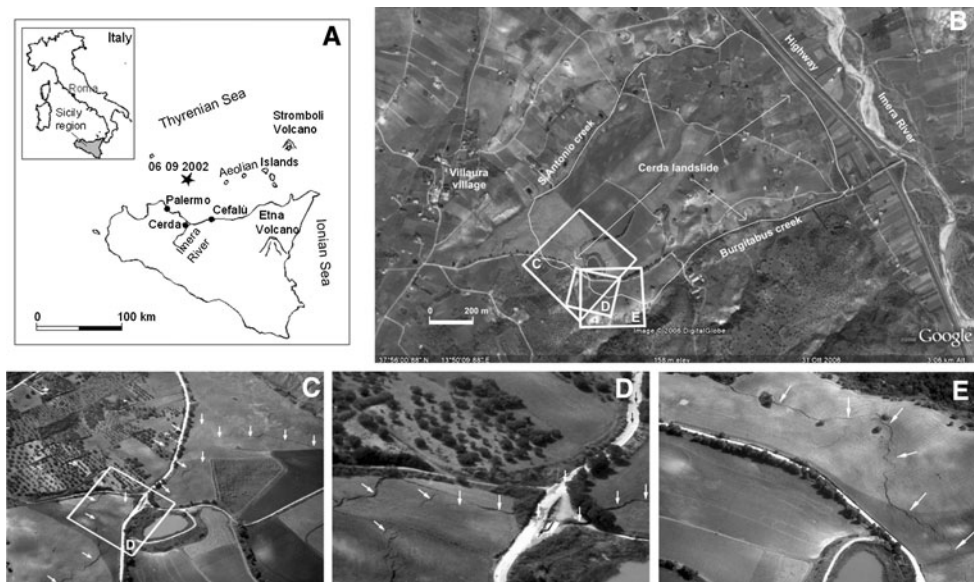
In order to take into account the amplification effects due to basin-like geological setting combined with pre-existing landslide masses, as well as the interactions between seismic inputs and slopes in terms of stability conditions, numerical modelling can be performed, via stress–strain approaches, by use of finite difference method (FDM) software. These approaches may benefit from a time-dependent force which takes into account both inertial effects due to the landslide mass movement and shaking effects due to the seismic input (Martino and Scarascia Mugnozza 2005; Martino et al. 2007). The used numerical codes (Bozzano et al. 2008c) allow a time-dependent non-linear incremental solution where dynamic properties (shear stiffness and damping) decay with shear strain.

## The Cerda landslide

### Geological setting of the Cerda landslide area

On 6th September 2002 an earthquake ( $M_s = 5.4$ ) occurred in the Tyrrhenian Sea, about 45 km NE from Palermo (Fig. 1a), at a depth of about 10 km. Notwithstanding the moderate magnitude, the event locally produced damage in Palermo city, due to the high vulnerability of the buildings

**Fig. 1** **a** Cerda landslide location (*star* corresponds to the 6th September 2002 earthquake epicentre); **b** GoogleEarth satellite view of the Cerda landslide area; **c–e** aerial view of ground cracks in correspondence with the detachment area of the Cerda landslide, some days after the triggering earthquake (courtesy of INGV)



or site-unfavourable conditions; 23 municipalities in the Northern coast of Sicily and the nearby hinterland suffered slight damages (Azzaro et al. 2004).

The Cerda landslide represents the main ground effect due to this earthquake (Fig. 1b); the landslide involved an area of about 1.5 km<sup>2</sup> and was characterised by a mainly translational mechanism (Cruden and Varnes 1996). It damaged many farmhouses, two aqueducts and some side roads. According to the witnesses, the activation of the landslide took place about 30 min after the main shock and within a couple of hours; most of the cracks had horizontal and vertical offsets up to 5 m (Fig. 1c–e), which were increased by the rainfall that occurred during the following 48 h.

The Cerda landslide mainly involved clay shales of the Argille Varicolori Formation (Cretaceous–Eocene) and marls and calcarenites of the Polizzi Formation (Eocene–Oligocene) (Fig. 2). The Argille Varicolori Formation

(Fig. 3a) overthrusts Triassic marls and limestones (Cerde-Roccapalumba Formation) (Fig. 3b), widely outcropping in a tectonic window SW of the Cerda landslide (Abate et al. 1988). The thrust limits the right side of the landslide mass, corresponding to the creek which bounds southward the landslide mass (Figs. 1, 2). The same thrust is offset by numerous tear faults; one of them partly corresponds to the main scarp of the landslide (Bonci et al. 2004).

The resulting structural setting of the slope is an open-basin-like structure, characterised by a high-angle lateral boundary upslope and by an irregularly shaped bedrock, whose top dips downhill (see geological section in Fig. 2).

The landslide mass is characterised by a large basal shear zone, composed of a 7-m-thick oxidised layer of clay shales, including a 2-m-thick layer of completely remoulded and oxidised clays. The depth of the sliding surface varies from zero (crown area) up to 60 m (toe of the

**Fig. 2** Geological map of the landslide area: 1 landslide mass, 2 alluvial deposits of the Imera River, 3 sandstones and sands of the Villaura Formation (Upper Miocene–Pliocene), 4 clay shales of the Argille Varicolori Formation (Cretaceous–Eocene), 5 calcarenites of the Polizzi Formation (Eocene–Oligocene); 6 marls and calcarenites of the Cerda–Roccapalumba Formation (Triassic), 7 alluvial fan, 8 pond dam, 9 thrust, 10 tear fault, 11 attitude of strata, 12 normal crack within the landslide mass, 13 inverse crack within the landslide mass, 14 crack within the landslide mass, 15 strike-slip crack within the landslide mass, 16 aqueduct, 17 borehole, 18 trace of geological section, 19 supposed top of the Cerda–Roccapalumba calcarenites and marls in the geological section, 20 kinematical indicators for tear faults in the geological section (*a* left fault, *b* right fault), 21 supposed bottom of the Imera River alluvial deposits in the geological section, 22 supposed thickness of the Argille Varicolori clay shales in the geological section

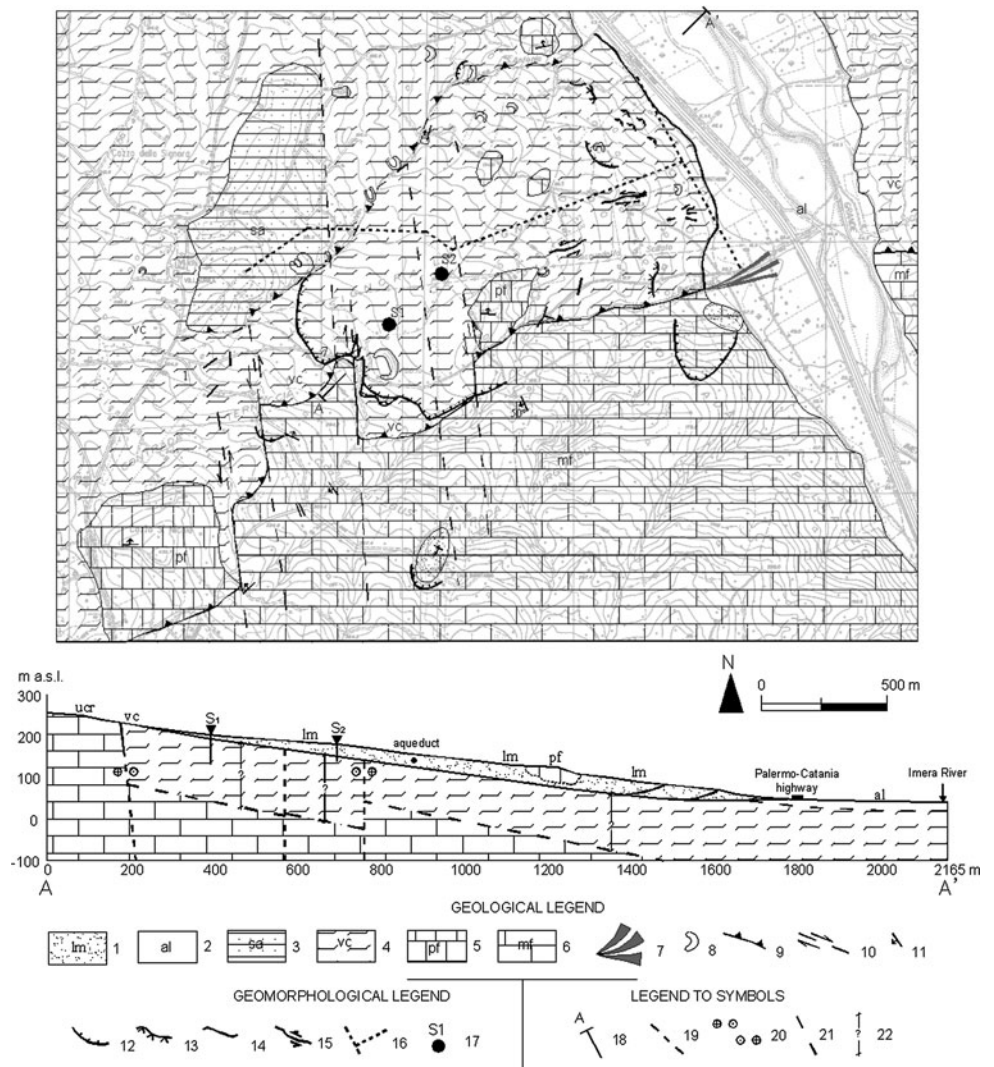




**Fig. 3** **a** Clay shales of the Argille Varicolori Formation which include calcarenites of the Polizzi Formation, outcropping NW to the Cerda landslide area. **b** Marls and calcarenites of the Cerda-Roccapalumba Formation outcropping SE to the Cerda landslide area

landslide) and was inferred from borehole data (Bozzano et al. 2004b, 2008b); this evidence is in agreement with the observed ground crack pattern. Though no historical documents testify past activations of the Cerda landslide, both thickness and oxidation of the remoulded clays in the shear zone testify its recurrent activity. Moreover, the S-wave profile inferred from cross-hole measurements shows a sharp velocity increase (from 400 up to 600 m/s) just below the sliding surface, where high-consistency and undisturbed clay shales were sampled (Bozzano et al. 2008a).

#### Seismicity of the Cerda landslide area

The seismicity of the Cerda landslide area was assessed from the available macroseismic data (CFTI3 2000; DBMI04 2004; CPTI04 2004; Castello et al. 2006): the maximum intensity historically observed at the site is VII MCS (Sieberg 1930), during the 5th March 1823 earthquake, which produced widespread damage all along the Tyrrhenian coast of Sicily. The 1823 macroseismic

epicentre is located on the coast; however, recent data (Gruppo di Lavoro 2004) suggest that the earthquake source could be located in a fault system E–W oriented, which extends west of the Aeolian arc as far as the Island of Ustica and which is also responsible for the 6th September 2002 event (Fig. 4a). As a consequence, most of the past seismic events can be referred to earthquakes which had their actual epicentre in the above-mentioned offshore source.

The earthquake source nearest to Cerda is the Madonie area (Agate et al. 2000; Giunta et al. 2004), with epicentral distances of 20–30 km and  $M_{aw} = 5.3$ –5.4 (i.e. 1818 and 1819 events). According to the collected data, the landslide site has no local seismicity and intensities as large as VII MCS can be expected, mainly due to the Tyrrhenian offshore source. Since seismometric records are not available for this source, in order to obtain the dynamic inputs for the numerical models, accelerometric data from the European Strong Motion Database (ESMD, Ambraseys et al. 2002) were used. In this regard, in agreement with the DISS3 catalogue (Basili et al. 2008), the considered accelerometric data are referred to the north-eastern Sicily area and to the Aeolian arc source (ITGG045 in the DISS3 catalogue, Fig. 4a) whose source parameter values (i.e.  $M_w$  and slip rate) are very close to the ones of the Tyrrhenian offshore source (ITGG056 in the DISS3 catalogue, Fig. 4a). Nevertheless, the fault mechanisms attributed to the two source areas are different, since a mainly compressive mechanism is attributed to the ITGG045 source while a mainly strike–slip mechanism to the ITGG056 one.

The 15th April 1978 Golfo di Patti earthquake ( $M_I = 5.0$ ) was selected from the ESMD database with regard to the representativeness of the records when compared with the reference one. It was recorded by four accelerometric stations, located up to about 44 km from the epicentre (Naso, Patti, Milazzo and Messinal, respectively, see Fig. 4a). The selected event can be considered as comparable to the 6th September 2002 Palermo earthquake in terms of PGA and magnitude. Nevertheless, in order to take into account the different fault mechanisms of the respective source areas, a PGA correction from strike to compressive was adopted, according to Bommer et al. (2003).

#### Dynamic FDM numerical modelling

Stress–strain 2D numerical modelling was carried out with the FLAC 5.0 (ITASCA 2005) FDM software in dynamic configuration. This modelling aimed at analysing the role of both seismic input and geological setting in triggering the Cerda landslide. For the numerical models, a  $340 \times 60$

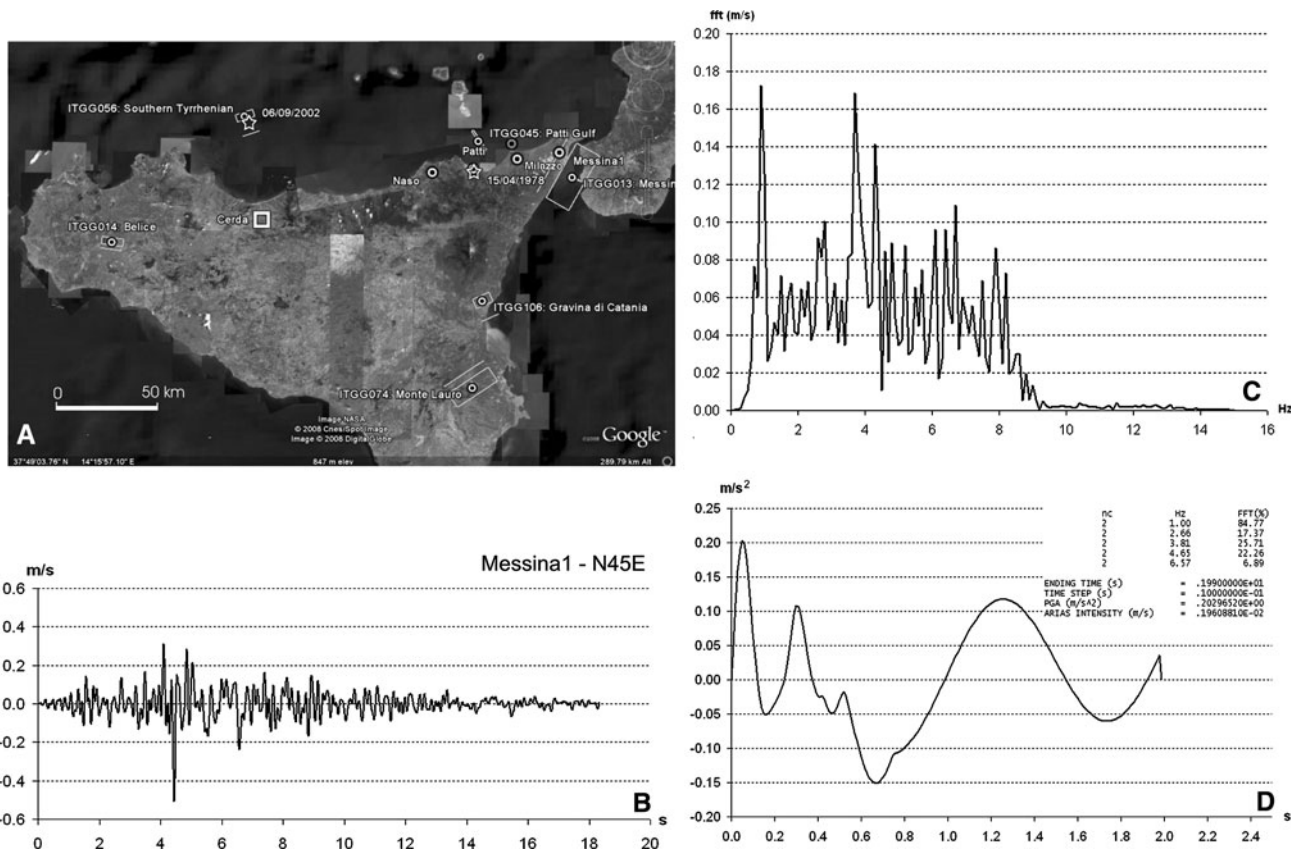


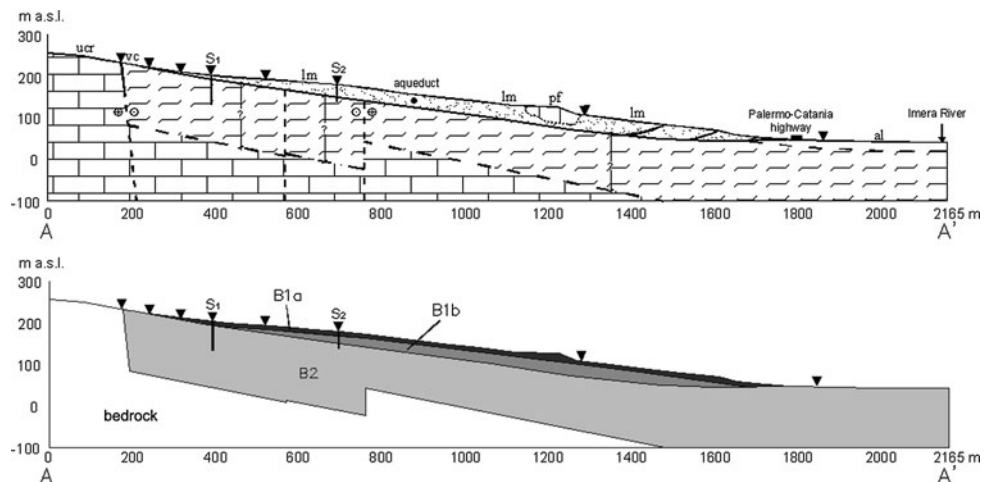
**Fig. 4 a** Epicentre location of 6th September 2002 Palermo earthquake and of the 15th April 1978 Golfo di Patti earthquake, seismogenic faults are also reported from DISS3 (Basili et al. 2008). **b** Accelerometric time history recorded at Messina1 station (see Fig. 4a for location) resulting in the sliding direction of the Cerda landslide. **c** Fourier spectrum of the acceleration time history of

**Fig. 4b. d** Dynamic equivalent input by LEMA\_DES 3.3 code obtained from the time history of Fig. 4b (table shows the main parameters and properties of the equivalent input: *nc* equivalent cycles, *FFT%* amplitude percentage of each selected frequencies in the equivalent input Fourier spectrum)

mesh with a 4-m<sup>2</sup> resolution was used, assuming the engineering-geology model of Fig. 5, obtained along section AA' of Fig. 2. As derived from the borehole stratigraphic logs, this model is composed of four zones: (1) a superficial debris of remoulded clays, up to 13 m thick; (2)

the landslide mass, composed of destructured clay shales (including the superficial debris) with a thickness varying up to 60 m; (3) the high-consistency clay shales located below the landslide mass; (4) the stiff bedrock composed of marly limestones.

**Fig. 5** Engineering-geology model of the Cerda landslide (top) and related physical model (bottom) along section AA' of Fig. 2 (labels B1a, B1b and B2 indicate the different “basin-like” geometries discussed in the text); the triangles on surface correspond to the noise recording stations. See Fig. 2 for legend to symbols



An elastic constitutive law was attributed to the geological bedrock, while a viscoelastic model was attributed to all the other simulated materials. Moreover, both *x*-displacements and *y*-displacements were permitted along the lateral boundaries.

Values of physical and mechanical parameters were derived from both laboratory tests on undisturbed samples and field geophysical investigations (Bozzano et al. 2004b, 2008a), taking into account their variation with in situ confining pressures (Table 1).

Initial equilibrium was obtained under the action of gravity only. During dynamic modelling, geotechnical deformational parameters were modified taking into account the decay of the dynamic shear modulus (*G*) versus the shear strain from dynamic laboratory tests (i.e. resonant column tests, performed at the Politecnico di Torino Geotechnical Laboratory) (Fig. 6). Mechanical dissipation was computed using a Rayleigh Damping function (Zienkiewicz 2005), adding a mass-dependent term to a stiffness-dependent one in the following form:

$$C = \alpha M + \beta K \tag{1}$$

where  $\alpha$  = constant for the mass damping (*M*) and  $\beta$  = constant for the stiffness damping (*K*). This dissipation function implies a minimum frequency in the form:

$$\left(\omega_{\min} = (\alpha/\beta)^{1/2}\right) \tag{2}$$

which gives a minimum damping in the following form:

$$\left(\xi_{\min} = (\alpha\beta)^{1/2}\right). \tag{3}$$

The damping  $\xi_{\min}$  values were modified during dynamic simulation according to the laboratory-derived curves of damping (*D*) versus shear strain (Fig. 6).

According to a traditional approach (Seed and Idriss 1969; Seed 1979; Martino and Scarascia Mugnozza 2005; Martino et al. 2007), equivalent dynamic inputs for numerical modelling and laboratory tests are defined as cyclic signals (i.e. sinusoidal functions), whose amplitude is derived from the PGA of a selected time history. In contrast, duration and energy content are not controlled, since the number of significant cycles is derived from the earthquake magnitude through an empirical relation and the frequency is not explicitly defined.

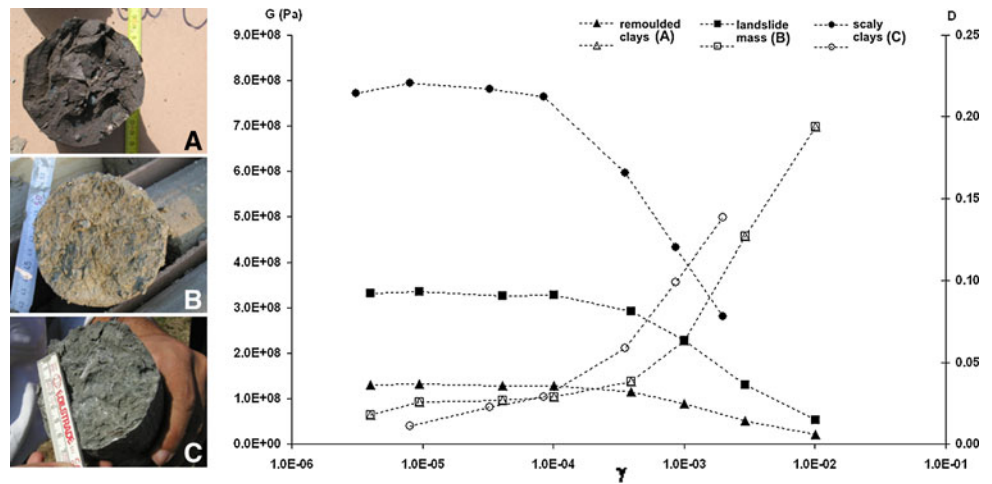
As a consequence, in order to control the frequencies as well as the energy content of the used equivalent inputs, a levelled-energy, multifrequencial, dynamic equivalent signal was obtained according to a new approach suggested by Lenti and Martino (2009). The equivalent accelerometric input (Fig. 4d) was derived from the time history of the 15/04/1978 earthquake,

**Table 1** Values of static and dynamic geomechanical properties adopted for both FLAC and INGV-WISA numerical models

FLAC	INGV-WISA	Constitutive law	Den (kg/m <sup>3</sup> )	<i>E</i> <sub>0</sub> (Pa)	<i>E<sub>r</sub></i> ( $\sigma_3$ ) (Pa)	<i>E<sub>s</sub></i> ( $\sigma_3$ ) (Pa)	$\nu$	<i>c</i> (Pa)	<i>Ten</i> (Pa)	<i>V<sub>s</sub></i> (m/s)	<i>G</i> <sub>0 dyn</sub> (Pa)
Remoulded clays B1a		Viscoelastic	2,100	1.49E + 08	9.00E + 07 <sup>e(1E-06)<math>\sigma_3</math></sup>	74.26 $\sigma_3$ + 2.00E + 06	0.25	17 0	0	250	1.31E + 08
Landslide mass B2b		Viscoelastic	2,100	1.49E + 08	9.00E + 07 <sup>e(1E-06)<math>\sigma_3</math></sup>	74.26 $\sigma_3$ + 2.00E + 06	0.25	17 0	0	400	3.36E + 08
Scaly clays B2		Viscoelastic	2,200	1.49E + 08	9.00E + 07 <sup>e(1E-06)<math>\sigma_3</math></sup>	74.26 $\sigma_3$ + 2.00E + 06	0.25	22 2.30E + 04	5.70E + 04	600	7.92E + 08
Marly limestones <i>Bedrock</i>		Elastic	2,400	1.00E + 10	-	-	0.25	-	-	-	-

*den* Density, *E*<sub>0</sub> initial modulus, *E<sub>r</sub>* elastic Young modulus, *E<sub>s</sub>* elasto-plastic secant modulus,  $\nu$  Poisson ratio,  $\phi$  friction angle, *c* cohesion, *Ten* tension cut-off; *V<sub>s</sub>* S-wave velocity from cross-hole measurement (Bozzano et al. 2008a, b, c), *G*<sub>0 dyn</sub> initial dynamic shear modulus

**Fig. 6** Dynamic shear modulus ( $G$ ) and adimensional damping coefficient ( $D$ ) versus shear strain ( $\gamma$ ) obtained from resonant column tests on borehole undisturbed samples of remoulded clays (a), destructured clay shales of the landslide mass (b), high-consistency clay shales of the Argille Varicolori Formation (c). Closed symbols are referred to  $G$  versus  $\gamma$  and open symbols to  $D$  versus  $\gamma$



recorded at Messina1 station (Fig. 4b) and has the following properties:

1. the frequency peaks of the FFT are in the range 1–8 Hz (Fig. 4c). These frequencies are consistent with the grid resolution, according to the relation  $f = Vs/10\Delta l$  (where  $f$  is the maximum admissible frequency of the model) (Kuhlemeyer and Lysmer 1973), where  $Vs$  = minimum velocity of S-waves and  $\Delta l$  = size of the largest mesh of the grid;
2. the energy content is set as equal to the one of the reference record;
3. the integration on the total time is equal to zero in order to avoid unjustified cumulative displacement;
4. PGA value ( $0.2 \text{ m/s}^2$ ) is consistent with the maximum expected in 475 years (INGV 2006) (Fig. 4d);
5. two representative cycles are derived for all the frequencies, in order to calibrate the equivalent PGA value with respect to the reference one (Fig. 4d);
6. an input duration of 2 s results from selected frequencies and the number of representative cycles; nevertheless, a simulation time up to 5 s was considered, since this value is sufficient for allowing damping and reaching a new static equilibrium in post-seismic conditions.

In the numerical modelling the soil damping was performed by assuming the following two conditions: (1) the  $\omega_{\min}$  value in the Rayleigh Damping function was considered equal to the frequency related to the highest peak in the FFT of the dynamic equivalent input, (2) a lateral infinite medium was reproduced by defining quiet boundaries, under free-field conditions. Under these assumptions, no boundary-reflection waves were generated within the model.

Before performing the dynamic numerical analysis, a yield pseudostatic acceleration  $a_y = 1.7 \text{ m/s}^2$  was computed according to the relation by Jibson (1993):

$$a_y = g \tan(\phi - \beta) \tag{4}$$

and assuming acceleration  $g = 9.81 \text{ m/s}^2$ , inclination ( $\beta$ ) =  $10^\circ$  and residual friction angle ( $\phi$ ) =  $16^\circ$ . The thus computed value cannot be directly compared to the seismic input PGA, since a large landslide mass is not simultaneously displaced in the same direction during a seismic shaking and, as a consequence, a part of it provides a stabilizing effect (Hutchinson 1987). Indeed, if this effect is taken into account, the effective equivalent pseudostatic PGA, acting within the whole landslide mass, results in a value significantly lower than the PGA value of the earthquake. As a consequence, in the case of the Palermo earthquake, starting from the estimated PGA of about  $0.1 \text{ m/s}^2$ , an equivalent pseudostatic PGA of  $0.06 \text{ m/s}^2$ , acting within the Cerda landslide mass, can be computed. Since this value is lower than the computed  $a_y$ , the back analysis of the Cerda landslide reactivation is not verified by performing a pseudostatic stability analysis.

In contrast, the stress–strain dynamic approach, performed by applying dynamic equivalent inputs with PGA values in the range  $0.1\text{--}0.2 \text{ m/s}^2$ , points out a reactivation of the pre-existing landslide. In particular, the reactivation occurs in correspondence with the tail of the equivalent input (i.e. in the time range 1–2 s), when only the lowest characteristic frequency occurs (Fig. 4d). Figures 7 and 8 clearly show a decay of the strain modulus all along the sliding surface at about 1.5 s after the beginning of the equivalent input. Moreover, in post-seismic conditions shear bands due to failure occur within the landslide mass in the detachment area (see Fig. 8d in the distance range 650–900 m from the left side of the model). In contrast, the landslide is not reactivated by the dynamic inputs, neither in co-seismic nor in post-seismic conditions, if, in the same numerical model, the marly limestone bedrock is not modelled and the high-consistency clay scales (Fig. 5) are zoned down to the model bottom (Fig. 9).

**Fig. 7** Dynamic numerical modelling by FLAC 5.0 code performed applying the dynamic equivalent input of Fig. 4d with a  $PGA = 0.1 \text{ m/s}^2$  along section AA' of Fig. 2

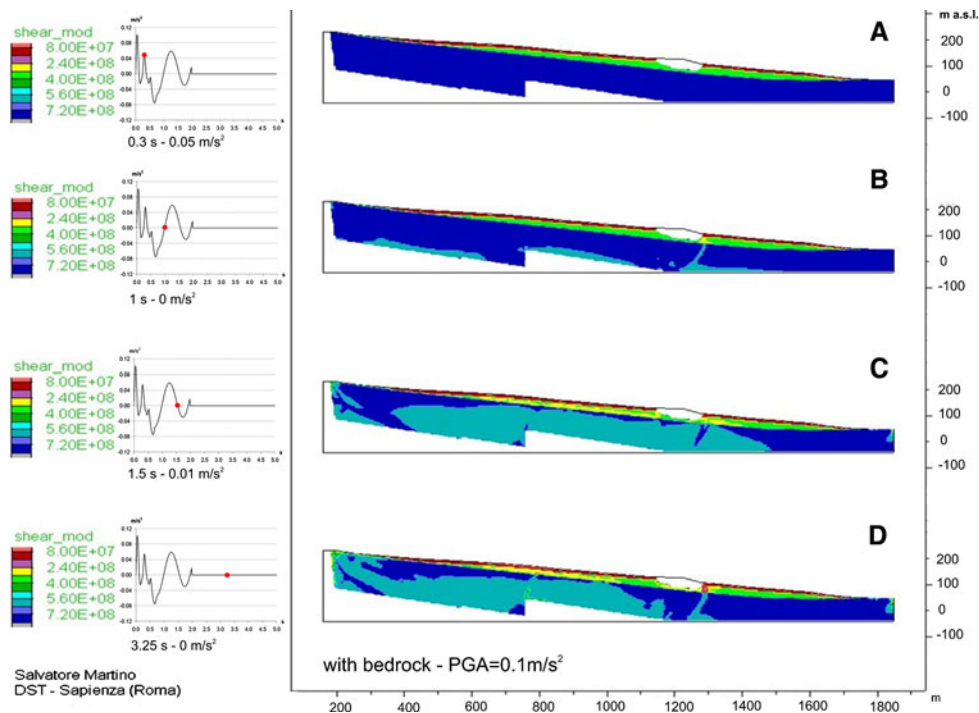
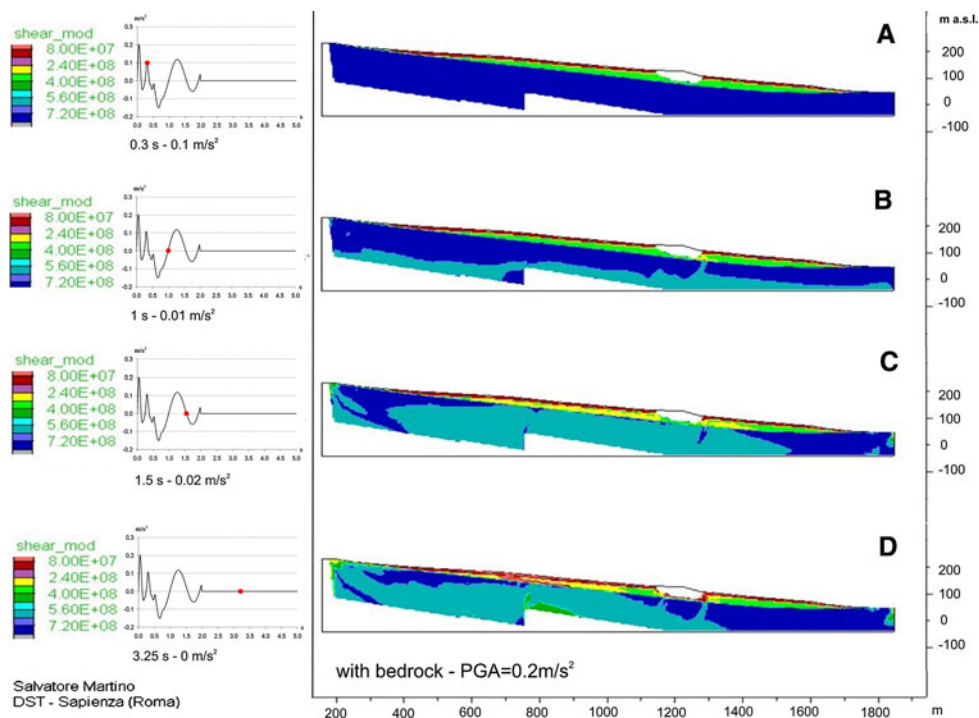


**Fig. 8** Dynamic numerical modelling by FLAC 5.0 code performed applying the dynamic equivalent input of Fig. 4d with a  $PGA = 0.2 \text{ m/s}^2$  along section AA' of Fig. 2

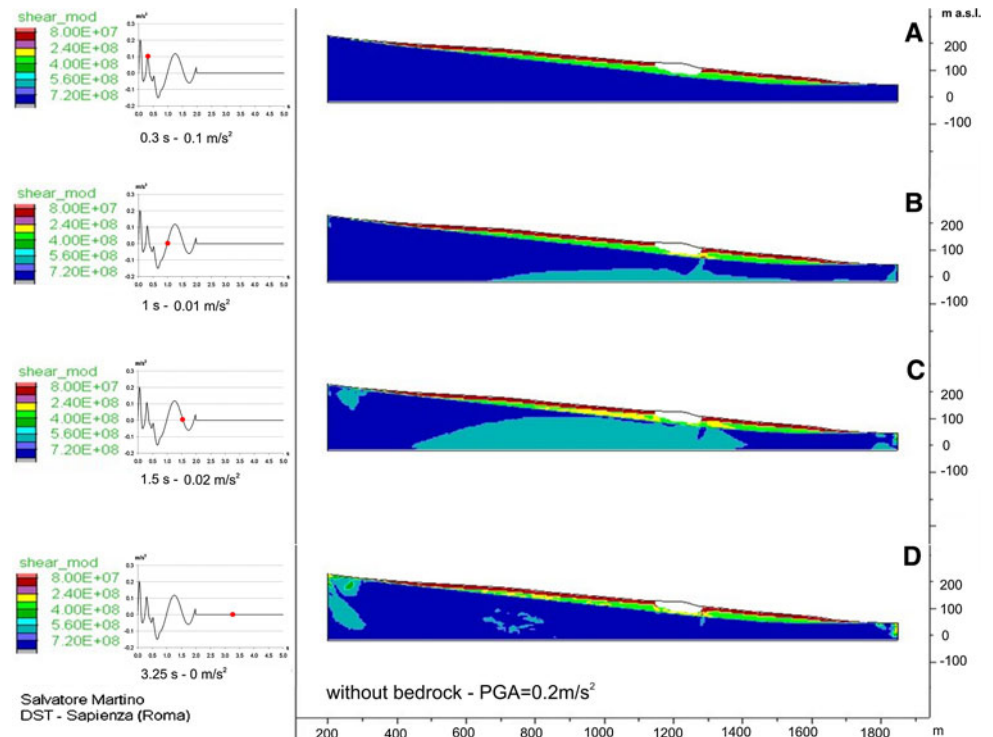


These results highlight the role of the frequency content of the triggering event as well as the geological setting of the bedrock. The analysis of the shear modulus decay resulting by the dynamic numerical modelling and reported in Figs. 7, 8 and 9 points out that:

1. the low frequencies ( $< 2 \text{ Hz}$ ) are responsible for larger portions of the pre-existing landslide mass to be simultaneously displaced downhill (Figs. 7, 8);
2. the lowest characteristic frequency (1 Hz), acting at the tail of the dynamic input with an amplitude in the



**Fig. 9** Dynamic numerical modelling by FLAC 5.0 code performed applying the dynamic equivalent input of Fig. 4d with a  $PGA = 0.2 \text{ m/s}^2$  along section AA' of Fig. 2, without reproducing the basin-like setting of the stiff bedrock



range 0.05–0.1  $\text{m/s}^2$ , is responsible for failures within the landslide mass (Figs. 4d, 6, 7);

- the downhill dipping of the bedrock drives the seismic wave front parallel to the sliding surface of the landslide (compare Fig. 8c and Fig. 9c).

### Local seismic response analysis from in situ measurements and 2D numerical modelling

#### Velocimetric records

In order to point out local seismic amplification effects, in situ geophysical measurements as well as 2D numerical modelling of the seismic wave propagation were performed.

A velocimetric survey was carried out with the aim of analysing the local seismic response inside and outside the landslide area (Bozzano et al. 2008a). A moving station, equipped with a digital acquisition unit (K2 Kinematics) and three short-period seismometers (SS1 Kinematics) triaxially arranged (NS-UP-WE), was used to record ambient noise samples. While noise measurements were performed, a temporary velocimetric array was deployed to record possible small-magnitude events. Three free-field stations (respectively S1, S2 and R in Figs. 2, 10), also in this case each one instrumented with a K2 digital acquisition unit, three SS1 seismometers and GPS for absolute

timing, operated for 10 days (24/06/2006–02/07/2006) in short time amplitude/long time amplitude (STA/LTA) acquisition mode. According to Borchardt (1994), a “reference station” (R) was positioned outside the landslide mass, on the outcropping stiff bedrock, on a flat site with no evidence of intense rock mass jointing; the other two stations were located on the landslide mass.

Since only two weak motions were recorded by the temporary velocimetric array (at stations S1 and S2 and at stations S1 and R, respectively), the analysis of the seismic response was mainly based on the ambient noise records, according to the horizontal/vertical spectral ratios (HVSr) Nakamura (1989) technique. The obtained HVSr (Bozzano et al. 2008a) point to a wide amplifying zone in the range 0.5–1 Hz within the landslide mass, up to about 500 m from the detachment area (Fig. 10). Along the landslide perimeter zone, the amplified frequencies are in the range 2.5–4.5 Hz, while they reach values of up to 7.5 Hz inside the landslide mass, near to its toe (Fig. 10).

Only at station S1 the receiver functions (Field and Jacob 1995) were obtained for both the recorded weak motions; at the same station, it was possible to compute the spectral ratio to the reference station R only for one of the two recorded events (Fig. 11). The results are consistent with those obtained from the HVSr of ambient noise and point out local amplification effects in the narrow frequency range 0.5–1.5 Hz as well as in the wide frequency band 2.5–5 Hz (Figs. 10, 11).

**Fig. 10** Frequencies corresponding to the maximum HVSR values in the Cerda landslide area; *circles* mark the recording stations for ambient noise, while *squares* mark the temporary velocimetric array stations: 1 landslide mass, 2 thrust, 3 tear fault, 4 borehole (S1 and S2)

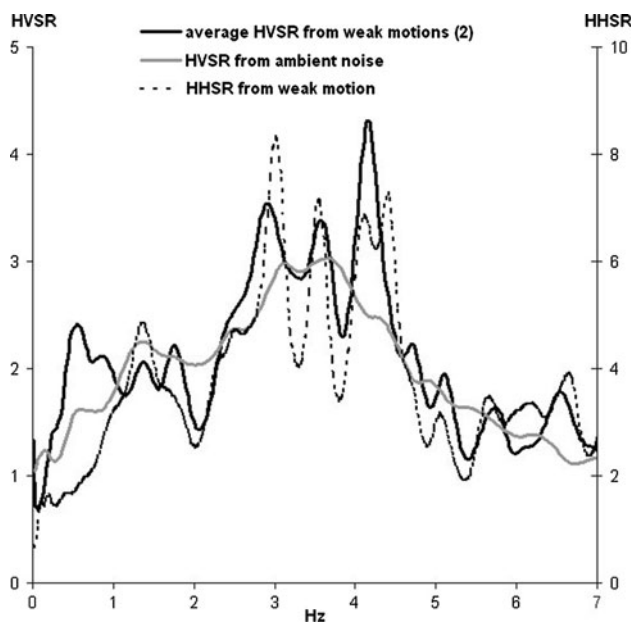
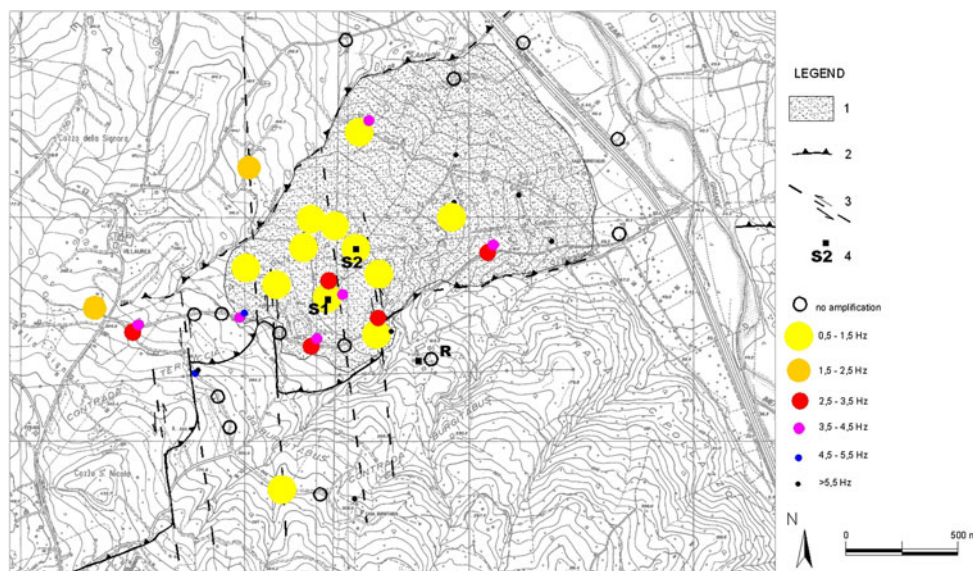


**Fig. 11** HVSR from both ambient noise and weak motions recorded at station S1 (see Fig. 9 for location) of the velocimetric temporary array installed in the Cerda landslide slope and average HHSR to the reference station R

## 2D numerical modelling

A 2D numerical simulation of seismic wave propagation in correspondence with the Cerda landslide slope was also performed according to the engineering-geology model of Fig. 5. Nevertheless, in order to analyse the obtained results this model can be transposed in a physical one including two basins with significantly different dimensions (Fig. 5): a smaller and shallower basin, representing the landslide mass (B1), and a larger and deeper basin, constituted of clay shales embedded in the marly and

calcarenitic bedrock (B2). Moreover, the B1 basin is split in two layers, which, respectively correspond to the 13-m-thick layer of superficial remoulded clays (B1a) and to the landslide mass, with an increasing thickness up to 60 m b.g.l (B1b).

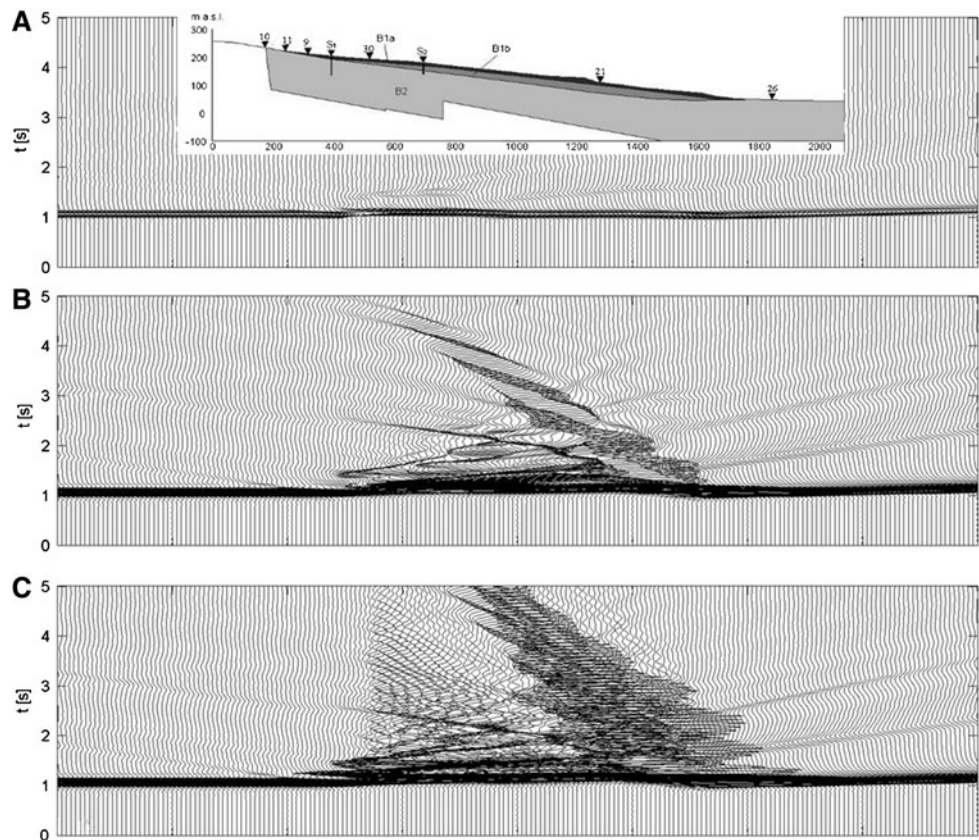
Three different 2D models were performed by the INGV-WISA (a proper linear wave propagation code by Italian Institute for Geophysics and Volcanology) software (Caserta et al. 2002; Santoni et al. 2004) in order to separately analyse the role of the two basins in the adopted physical model. For all the simulations, the numerical model was divided into a  $392 \times 799$  grid representing a 1,400-m-deep and 9,000-m-long rectangular domain. The maximum spatial step  $\Delta l$  was equal to 1 m and the temporal one ( $\Delta t$ ) to  $4.9 \times 10^{-4}$  s. The corresponding maximum admissible frequency of the model,  $f = Vs/10\Delta l$  (Kuhlemeyer and Lysmer 1973), always lies well above 15 Hz. At the bottom of the model, the input was given in the form of a vertical upward SH-antiplanar wave, represented by a delta-like Gabor function  $G(t)$  having the following analytical expression:

$$G(t) = e^{-\left[\frac{2\pi f_p(t-t_s)}{\mu}\right]^2} \cos[2\pi f_p(t-t_s) + \varphi] \quad (5)$$

where  $\mu = 0.066$  is a coefficient related to the frequency range of the FFT,  $f_p = 0.45$  is the central frequency value of the FFT,  $t_s = 0.066$  is a value for time-translation and  $\varphi = \pi/2$  is the phase parameter. The choice of the latter parameters ensures a  $G(t)$  FFT with negligible spectral amplitudes for frequencies higher than 15 Hz. To avoid numerical errors during dynamic calculation, the function has a symmetrical shape and a null integral on the total time.

Since these simulations, differently from the already discussed simulations by FLAC, were performed under

**Fig. 12** S-wave propagation resulting from INGV-WISA numerical modelling in simulation I (a), II (b) and III (c), respectively; the comparison with the physical model of Fig. 5 is also shown (use distance values of the physical model as reference for  $x$ -axis)



linear conditions (i.e. elastic behaviour), damping ( $\zeta$ ) of the soils was represented by a linear viscoelastic constitutive law model, in which a nearly constant quality factor ( $Q = 0.5/\zeta$ ) for soils was introduced (Liu et al. 1976).

In simulation I the large scale basin with embedded Argille Varicolori (B2) was only considered (Fig. 5). The shear wave velocity was set at 990 m/s and the  $Q$  value at 10, as suggested by the values recorded within undisturbed fissured clay shales (Bozzano et al. 2008a). For the underlying half-space, a shear wave velocity of 1,450 m/s and a  $Q$  value of 50 were hypothesised. The two other simulations (II and III) took into account also the landslide basin (B1). In simulation II, the B1 basin was modelled by one layer corresponding to the whole landslide mass; in simulation III, the same B1 basin was simulated by 2 layers (B1a and B1b) representing the landslide mass and the superficial remoulded clays. The landslide basin (B1) was always boxed in the geological basin (B2) and the same half-open-space was considered. The spectral outputs obtained from the displacement time histories were filtered with a low-pass filter (<15 Hz).

The wave propagation obtained along the entire horizontal profile at the surface is shown in Fig. 12. However, the maximum dimensions of the largest basin were smaller than those of the overall simulated domain; this choice was made to avoid effects associated with numerical lateral

reflections in the synthetic outputs. The generation of Love surface waves was concentrated at the edges of the basins in all the simulations. The models including the landslide mass (B1a + B1b or B1b only) proved to alter the input motion much more significantly, since the resulting time histories (synthetics) have a longer duration and a higher amplitude (Fig. 12b, c).

For all the simulations, the outputs obtained at the model surface along the entire horizontal domain were FFT transformed. The reference grid point on outcropping bedrock was placed half way between the left boundary of the model and the left edge of the B2 basin. The spectral ratios to the reference grid point define the amplification function ( $A(f)$ ) and were obtained for the synthetic displacements all along the AA' section. The spectral ratios from simulation I indicate that the B2 basin contribute to amplifying the input motion (Fig. 13) at low frequencies (lower than 2 Hz); on the contrary, simulations II and III demonstrate the relevant role of the landslide mass in inducing amplification effects in the frequency range 3–5 Hz (Figs. 14, 15). Within this range the value of amplified frequencies gradually decrease moving downhill, in relation with the increasing thickness of the landslide mass.

In simulations II and III, the  $A(f)$  has a more complex configuration and a greater number of narrow and adjacent frequency peaks. The amplitude of the peaks values for

**Fig. 13**  $A(f)$  function obtained for simulation I by INGV-WISA numerical modelling (the effect due to basin-like geological setting of the bedrock is shown)

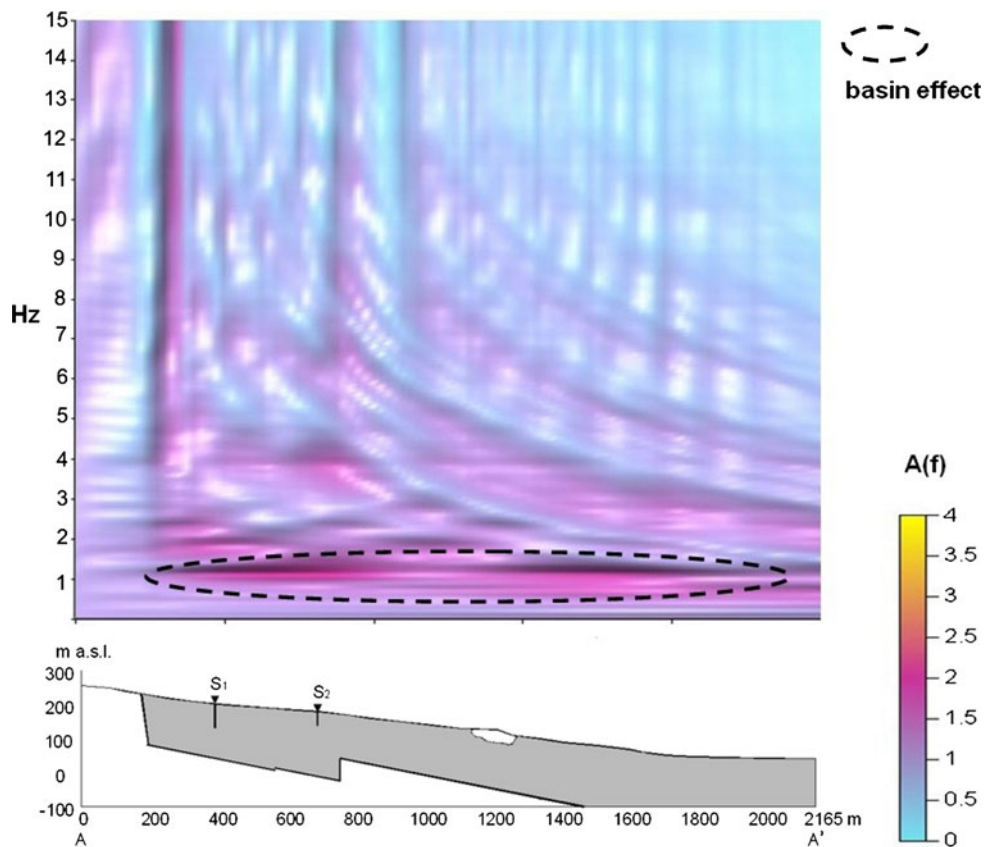


**Fig. 14**  $A(f)$  function obtained for simulation II by INGV-WISA numerical modelling (effects due to basin-like geological setting of the bedrock as well as to the pre-existing landslide mass are shown)

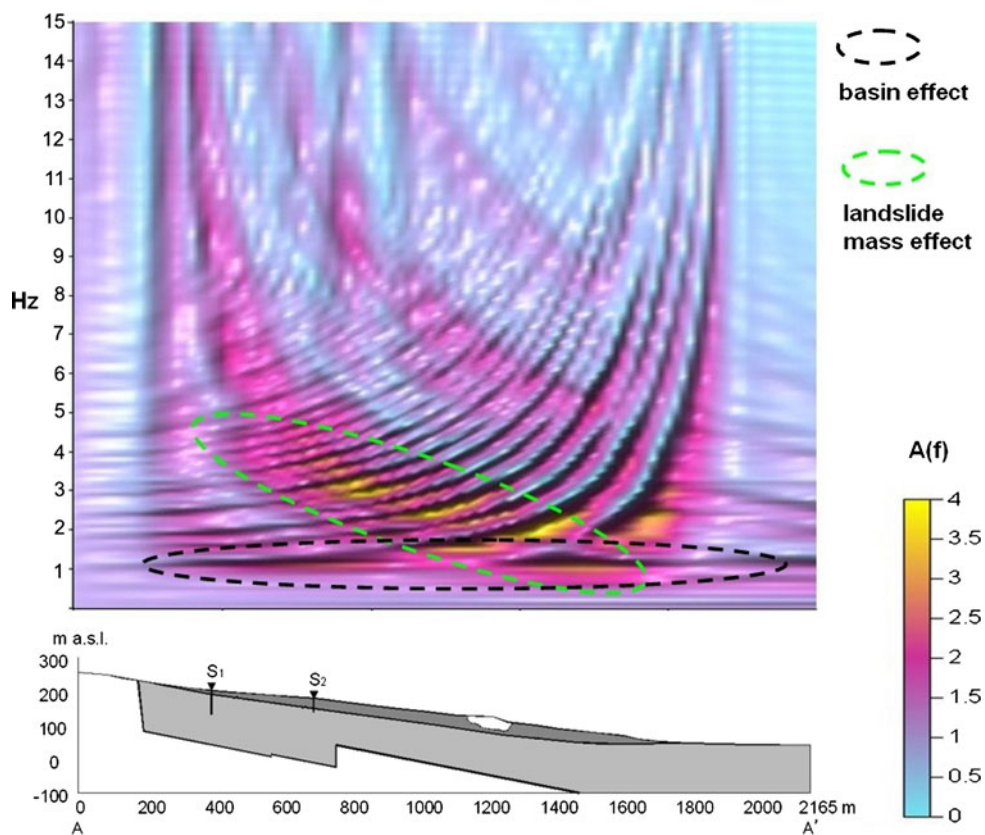
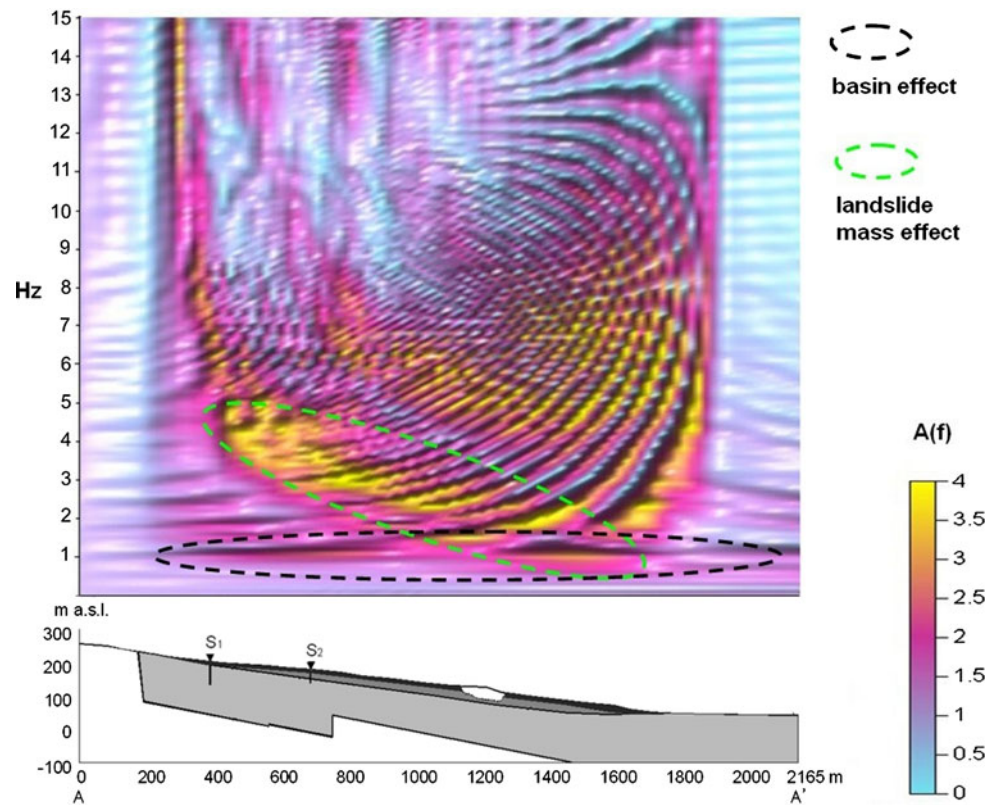


**Fig. 15**  $A(f)$  function obtained for simulation III by INGV-WISA numerical modelling (effects due to basin-like geological setting of the bedrock as well as to the pre-existing landslide mass are shown)



these simulations result to be up to two times higher than for simulation I.

In particular, in simulation I the  $A(f)$  amplitude is up to 2.5 at 1 Hz all along the slope; since the landslide mass is not considered, this effect can be related to the geological setting of the bedrock (Fig. 13); in simulation II the  $A(f)$  amplitude reaches a value of about 4 in the 2–4 Hz frequency range (Fig. 14) and the  $A(f)$  amplitude increases up to 3 at 1 Hz; in simulation III the  $A(f)$  amplitude increases up to 4 for all the amplified frequencies (Fig. 15).

Based on the modelling results by INGV-WISA code, the contributions of both geological setting and landslide mass can be distinguished in the local seismic amplification. In particular, the seismic response related to the bedrock is characterised by an almost constant value of the  $A(f)$  at 1 Hz while, on the contrary, the frequencies amplified by the pre-existing landslide mass decrease downhill with the increase of the landslide mass thickness. Moreover, the existence of the double-layered landslide mass within the half-opened basin-like system (B2) is responsible for a significant increase of the  $A(f)$  amplitude (Fig. 16a).

A 2D numerical modelling of the local seismic response in correspondence with the Cerda landslide slope was performed also by FLAC 5.0 adopting a FDM linear-equivalent incremental solution (Havenith et al. 2002, 2003a, b; Bourdeau 2005) and assuming the same

engineering-geology model for the above discussed dynamic stability analysis (Fig. 5).

With this aim, the previously defined delta-like Gabor function ( $G(t)$ ) was scaled to be energy-equivalent to the acceleration time history of the main shock and it was applied to the lower boundary of the model.

Also in this case, an amplification function  $A(f)$  was defined as spectral ratio between the FFT from the synthetics on the slope surface (at S1 position, see Fig. 2 for location) and the FFT of the outcropping bedrock (Fig. 16b). The computed  $A(f)$  function is characterised by a narrow frequency peak in the range 1–2 Hz and a large peaked band in the range 3–6 Hz.

The comparison among the  $A(f)$  function by INGV-WISA simulations and the HHSR obtained at S1 from velocimetric records proves that simulation III best fits the site effects, since both a narrow peak at low frequencies (about 1.5 Hz) and a large band at higher frequencies (range 3–6 Hz) are computed. In contrast, simulations I and II only point out the low-frequency peak, mainly related to the geological setting of the bedrock. Moreover, outputs at point S1, obtained from simulation III by INGV-WISA code, are in good agreement with the  $A(f)$  function obtained by FLAC code, when the geological bedrock is modelled (Fig. 16b).

Since no amplification effects result from ambient noise records in correspondence with the toe of the Cerda

**Fig. 16** **a** Comparison between  $A(f)$  functions obtained from numerical models by INGV-WISA and HHSR resulting from the two recorded weak motions at point S1 (see Figs. 2, 11 for location). **b** Comparison among  $A(f)$  functions obtained by INGV-WISA and by FLAC numerical models and HHSR resulting from the two recorded weak motions at point S1 (see Fig. 10 for location)

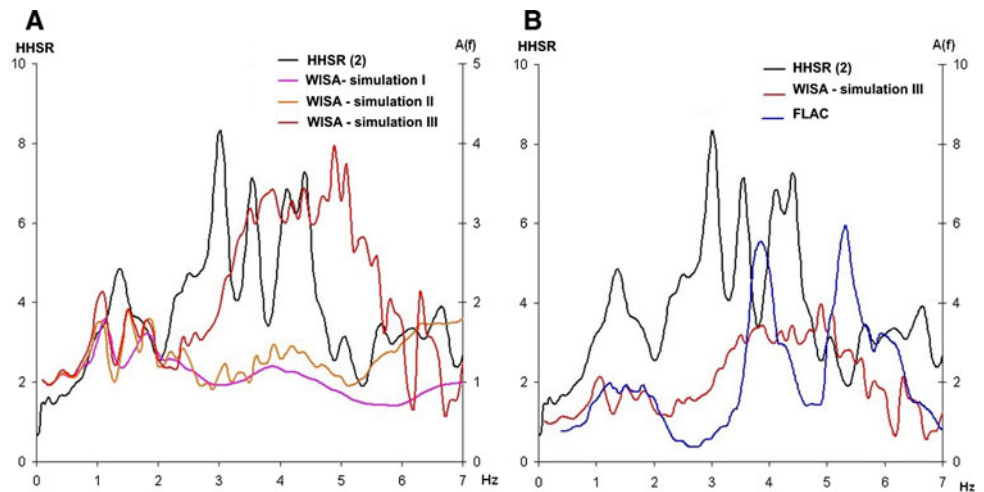
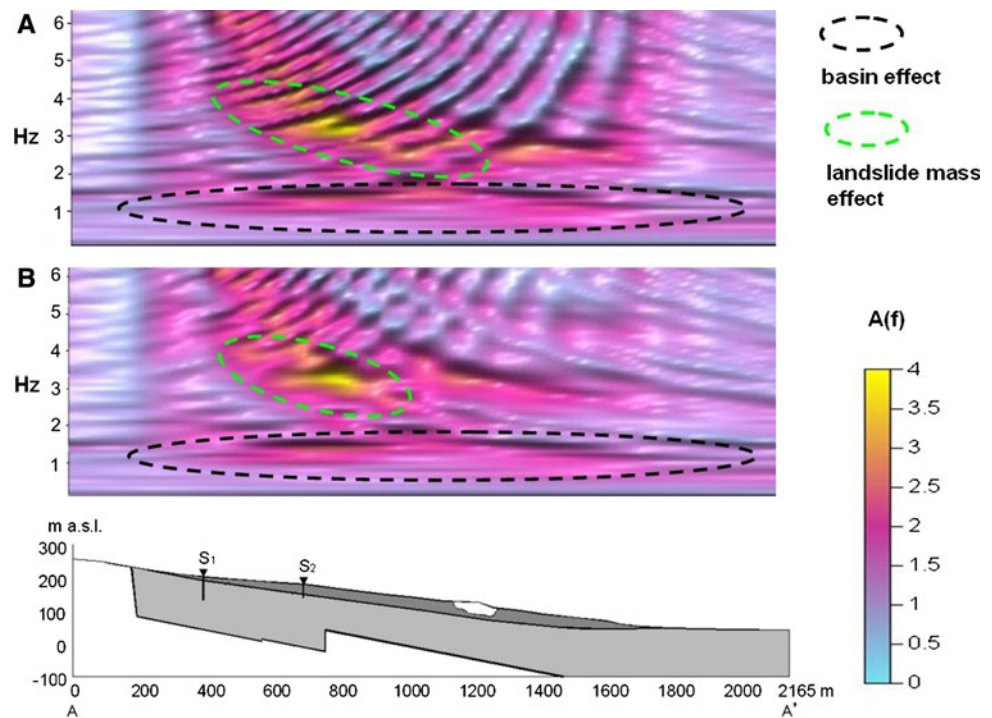


**Fig. 17**  $A(f)$  function obtained by INGV-WISA numerical modelling reducing downhill the S-wave velocity contrast along the landslide sliding surface up to 30% (**a**) and 70% (**b**), respectively (effects due to basin-like geological setting of the bedrock as well as to the pre-existing landslide mass are shown)



landslide, a lowering of the S-wave velocity contrast along the sliding surface can be assumed. It was simulated through the INGV-WISA code, splitting the landslide mass in eight slices, bounded by vertical limits, and lowering the S-wave velocity contrast downhill up to 30% (simulation IIa) and 70% (simulation IIb) of its initial value (Fig. 17a, b, respectively). It was possible to adopt the geometrical condition of simulation II only, due to the resolution limits of the numerical model.

The obtained results are in better agreement with the areal distribution of the amplification effects observed from ambient noise HVSr (Fig. 10), since  $A(f)$  amplitudes

higher than 3 are computed in the 2–4 Hz frequency range only for the detachment area of the landslide (Fig. 17).

## Discussion

Interactions between seismic waves and slopes in terms of directivity as well as spectral response are often difficult to be analysed and explained (Bonamassa and Vidale 1991; Spudich et al. 1996). Nevertheless, these interactions can be relevant for landslide triggering (Havenith et al. 2003b; Del Gaudio and Wasowski 2007)

The herein discussed case history of the Cerda landslide shows very similar feature with respect to the one of the Salcito landslide (Italy) (Bozzano et al. 2008b, c), since the two landslides were triggered by far-field earthquakes in comparable geological conditions. In particular, the pre-existing landslide masses and the local structural setting can be regarded as responsible for amplification effects due to the high impedance contrast between clay shales and calcarenitic or marly bedrock as well as the basin-like geometries of such stiff bedrock (Bard and Bouchon 1985; Mozco and Bard 1993). For both case histories, 2D numerical modelling, performed by FDM software, verified these amplification effects also in non-linear conditions.

The results are in agreement with recent field experiments (Del Gaudio and Wasowski 2007), based on spectral HVSR analysis of weak motion records, which observed directional effects, related to seismic amplification within pre-existing landslide masses and distinguished from the topographic ones (Chavez-Garcia et al. 1996).

According to Hutchinson (1987), frequencies lower than 2 Hz propagate with an half wave-length of some hundred of metres within landslide masses having a S-wave velocity up to 500 m/s; this half wave-length can be regarded as the minimum portion of the landslide mass which can be simultaneously moved downhill, along the sliding direction.

A major content at low frequencies generally typifies the FFT of earthquake acceleration time histories recorded in far-field conditions; as a consequence, “far earthquakes” result particularly adapt for triggering large landslides, even though the related shaking amplitude is generally too low for inducing non-linear soil deformations. The 31/10/2002 main shock of the Molise earthquake, responsible for the Salcito landslide reactivation, is characterised by a 1 Hz peak in the Fourier spectrum with a peak ground acceleration (PGA) of about 0.005g recorded about 15 km far from the landslide area (Dipartimento della Protezione Civile 2004).

Nevertheless, on the basis of the obtained results from the two above-mentioned case histories, seismic amplification effects can locally increase the PGA so as to induce the landslide reactivation. As a consequence, landslides involved in past activations (i.e. reactivated landslides, according to Hutchinson 1988) become prone to be seismically induced, since their masses can produce significant amplification effects at frequencies consistent with their size and their sliding mechanisms.

The resulting self-excitation process can be regarded as a local seismic amplification due to both structural setting of the stiff bedrock and pre-existing landslide masses, capable to produce seismically induced landslide reactivation. Even though such a process can also occur close to the earthquake epicentres in addition to other significant

shaking-induced effects (i.e. increasing of pore pressures, liquefaction, high PGA values) (Tiwari et al. 2008), it seems suitable to justify the far-field reactivations of large landslides at epicentral distances greater than those expected according to the mentioned distance versus magnitude empirical correlations (Keefer 1984; Rodriguez et al. 1999).

In this regard, given its large epicentral distance (about 50 km) and the moderate magnitude of the Palermo earthquake ( $M_s = 5.4$ ), the Cerda landslide considered here is well beyond the upper bound defined by the curve (Rodriguez et al. 1999), representing the maximum expected distance for activation of coherent landslides.

Dynamic numerical modelling as well as in situ geophysical measurements referred to the slope involved by this seismically induced landslide, pointed out the relevant role of both local geological setting and frequency content of the triggering input in justifying the far-field reactivation. In particular, the FDM numerical analysis, performed by FLAC code in dynamic configuration, demonstrated that the low-frequency content ( $<2$  Hz) of the triggering event and a PGA value representative of the local expected ground shaking (i.e. ranging from 0.1 to 0.2  $m/s^2$ ), is responsible for a relevant decay of the shear modulus along the sliding surface in co-seismic conditions as well as for failures within the landslide mass in post-seismic conditions. However, if the stiff bedrock is not reproduced in the model, the landslide reactivation does not occur; this finding highlights the significant role played by the geological setting of the slope.

In addition, the modelling of seismic wave propagation by INGV-WISA code made it possible to observe that low frequencies ( $<2$  Hz) are amplified by the stiff bedrock due to its basin-like setting; in contrast, higher frequencies (in the range 3–6 Hz) are amplified by the pre-existing landslide mass. Since the 1 Hz frequency results to be peaked in the FFT of the reference seismic event capable for triggering the landslide as well as in the  $A(f)$  function, which was numerically computed in correspondence with the landslide slope, the amplification at 1 Hz can be regarded as responsible for the seismically induced failures within the landslide mass, also in agreement with the performed dynamic slope stability analysis.

On the basis of the data collected for the Cerda landslide case history, no pore pressures are taken into account in the performed FDM numerical models since: (1) no groundwater flow was observed within the landslide slope neither during the geological in situ surveys nor during the performed boreholes; (2) rainfall only occurred during the 48 h following the landslide reactivation. As a consequence, the resulting post-seismic plasticization of the landslide mass and the associated ground failures are due to

ongoing inertial movements which started during the co-seismic phase, i.e. during the seismic shaking.

More in general, the findings obtained here highlight that ground evidences of displacements within seismically induced landslide masses, delayed with respect to the co-seismic phase (i.e. tertiary displacements according to Ambraseys and Srbulov 1995), are not necessary referable to post-seismic consolidation processes, i.e. due to the dissipation of exceeding pore pressures, but they can also result from seismically induced deformations of the landslide mass which leads to yielding conditions in the post-seismic phase.

Multidisciplinary investigations, devoted to obtaining a specific engineering-geology model, and including in situ geophysical measurements (Havenith et al. 2002, 2003a, b; Meric et al. 2005, 2007; Bièvre et al. 2008) as well as numerical modelling, seem to be the best approach to recognise and analyse the effects of the above-mentioned self-excitation process, strongly controlled by both local geological setting of stiff bedrocks and frequency content of triggering events.

In this regard, according to many experimental data (Steimen et al. 2003; Roten et al. 2004; Lenti et al. 2009), also fast seismometric techniques, such as Nakamura HVSR, are often able to reveal local amplifications due to both 1D and 2D effects, even if better information can be derived from weak or strong motion records. On the other hand, dynamic numerical modelling of self-excitation processes need major constraints in terms of both frequency and energy content of the applied input, suggesting new analytical approaches (Lenti and Martino 2009) to derive equivalent signals consistent with the seismic input to be modelled.

## Conclusions

The self-excitation process, capable of far-field reactivation of large landslides, can be defined as a peculiar seismic amplification effect, resulting from both structural setting of stiff bedrock and pre-existing landslide mass. Two Italian case histories (Salcito and Cerda landslides) proved such an effect by experiencing a multidisciplinary approach, which includes information deriving from engineering-geology field evidences, in situ geophysical investigations and numerical modelling (Bozzano et al. 2008b).

Based on the above-mentioned case histories, the self-excitation process results to be conditioned by: (1) basin-like structural setting of stiff bedrock; (2) a pre-existing landslide mass; (3) consistence among dimension of the basin-like structure of the stiff bedrock, size of the landslide and frequency content of the triggering event.

Moreover, it is possible to state that pre-existing landslide masses, typified by residual strength values and wide shear zones (Tika et al. 2008), are more susceptible to the previously defined self-excitation process.

When these conditions are satisfied, the combined effect of the 2D amplification of the basin and the 1D resonance of the pre-existing landslide mass can significantly increase the PGA values, favouring the landslide reactivation.

The self-excitation processes should be taken into account for seismically induced reactivation of landslides in highly tectonised geological areas, i.e. close to thrust faults or graben, when basin-like setting of stiff rocks constitute the bedrock of deep deposits characterised by lower stiffness and viscoplastic behaviour.

Based on the analysed case histories as well as on the previous considerations, landslides which are beyond the upper bound defined by the empirical curves representing the maximum distance for activation (Keefer 1984; Rodriguez et al. 1999) could be considered as far-field reactivation of self-excited landslide masses. Since these “outlier” events are not so easy to be forecast, they require a particular attention in the aim of risk mitigation.

Self-excitation processes can be expected also in near-field conditions, related to: (1) near earthquake, (2) major content at high frequencies ( $>2$  Hz) of the FFT-acceleration, (3) small landslide masses. Nevertheless, these events are not “outliers”, with respect to the above-cited empirical correlation, representing the maximum distance for activation versus magnitude and, for this reason, they can actually be forecast without taking into account possible self-excitation processes.

On the contrary, according to both Salcito and Cerda Italian “outlier” events, the self-excitation process extends maximum epicentral distance for seismically induced landsliding. Moreover, as demonstrated by the above-mentioned case histories, the far-field seismically induced landslides can widely involve large infrastructures (such as pipelines, gasducts, roads, highways) as well as extended urban areas. As a consequence, these “outlier” landslide events can be responsible for enlarging the high-risk zone associated with seismically induced ground effects.

**Acknowledgments** The Authors are indebted to D. Jongmans for his helpful suggestions and oral communications; to M. R. Manuel and F. Lucenti for their contribution to field investigations; to S. Porfido and E. Esposito for their contribution to the analysis of historical seismicity. Thanks also to the Italian National Institute for Geophysics and Vulcanology (INGV) for permitting the use of the INGV-WISA code. This research study was funded as part of the PRIN2005 national project “Induced seismic hazard: analysis, modelling and predictive scenarios of earthquake triggered landslides” (Project Leader: G. Scarascia Mugnozza).



## References

- Abate B, Renda P, Tramutoli M (1988) Schema geologico dei Monti di Termini Imerese e delle Madonie Occidentali (Sicilia). *Mem Soc Geol Ital* 41:465–474
- Agate M, Beranzoli L, Braun T, Catalano R, Favali P, Frugoni F, Pepe F, Smriglio G, Sulli A (2000) The 1998 offshore NW Sicily earthquakes in the tectonic framework of the southern border of the Tyrrhenian Sea. *Mem Soc Geol Ital* 55:103–114
- Ambraseys N, Srbulov M (1995) Earthquake induced displacements of slopes. *Soil Dyn Earthq Eng* 14:59–71. doi:10.1016/0267-7261(94)00020-H
- Ambraseys N, Smit P, Sigbjornsson R, Suhadolc P and Margaris B (2002) Internet-site for European strong-motion data, European Commission, Research-Directorate General, Environment and Climate Programme. On-line web site: <http://www.isesd.cv.ic.ac.uk/ESD/frameset.htm>
- Azzaro R, Barbano MS, Camassi R, D'Amico S, Mostaccio A, Piangiamore G, Scarfi L (2004) The earthquake of 6 September 2002 and the seismic history of Palermo (Northern Sicily, Italy): implications for the seismic hazard assessment of the city. *J Seismol* 8:525–543
- Bard PY, Bouchon M (1985) The two-dimensional resonance of sediment-filled valleys. *Bull Seismol Soc Am* 75:519–541
- Basili R, Valensise G, Vannoli P, Burrato P, Fracassi U, Mariano S, Tiberti MM, Boschi E (2008) The database of individual seismogenic sources (DISS), version 3: summarizing 20 years of research on Italy's earthquake geology. *Tectonophysics* 453:20–43. doi:10.1016/j.tecto.2007.04.014. On-line web site: <http://legacy.ingv.it/DISS/>
- Bièvre G, Delacourt C, Jongmans D, Kniess U, Orenge Y, Pathiern E, Renalier F, Schwartz S, Villemin T (2008) Characterization of the Avignonet landslide (French Alps) with seismic techniques. In: Chen et al (eds) *Landslides and engineered slopes*. Taylor and Francis Group, London. ISBN:978-0-415-41196-7:395-401
- Bird JF, Bommer JJ (2004) Earthquake losses due to ground failure. *Eng Geol* 75:147–179
- Bommer JJ, Douglas J, Strasser FO (2003) Style-of-faulting in ground-motion prediction equations. *Bull Earthq Eng* 1(2):171–203
- Bonamassa O, Vidale JE (1991) Directional site resonances observed from aftershocks of the 18th October 1989 Loma Prieta earthquake. *Bull Seismol Soc Am* 81:1945–1957
- Bonci L, Bozzano F, Calcaterra S, Eulilli V, Ferri F, Gambino P, Manuel MR, Martino S, Scarascia Mugnozza G (2004) Geological control on large seismically induced landslides: the case of Cerda (Southern Italy). In: *Proc IX ISL, Rio De Janeiro*, pp 985–991
- Borcherdt RD (1994) Estimates of site-dependent response spectra for design (methodology and justification). *Earthq Spectra* 10:617–653
- Bordoni P, Cara F, Cercato M, Di Giulio G, Haines AJ, Milana G, Rovelli A, Ruso S (2006) The use of a very dense seismic array to characterize the Cavola, Northern Italy, active landslide body. In: *Third international symposium on the effect of surface geology on seismic motion*, Grenoble, France
- Bourdeau C (2005) Effets de sites et mouvement de versants en zones sismiques: apport de la modélisation numérique. Unpublished PhD thesis, Mines, Paris
- Bozzano F, Cardarelli E, Cercato M, Manuel M.R, Martino S, Scarascia Mugnozza G (2004a), Determinazione delle proprietà dinamiche delle formazioni coinvolte nella frana di Salcito (CB) del 31 Ottobre 2002 tramite prove geofisiche in sito e prove di laboratorio. *Proc 23° Convegno Nazionale del Gruppo Nazionale di Geofisica della Terra Solida (GNGTS)*, pp 104–107
- Bozzano F, Martino S, Naso G, Prestininzi A, Romeo RW, Scarascia Mugnozza G (2004b) The large Salcito landslide triggered by the 31st October 2002, Molise earthquake. *Earthq Spectra* 20(2):1–11
- Bozzano F, Cardarelli E, Cercato M, Lenti L, Martino S, Paciello A, Scarascia Mugnozza G (2008a) Engineering-geology model of the seismically induced Cerda landslide. *Bollettino di Geofisica Teorica ed Applicata* 49(2):205–226
- Bozzano F, Lenti L, Martino S, Paciello A, Scarascia Mugnozza G (2008b) Self-excitation process due to local seismic amplification and earthquake-induced reactivations of large landslides. In: Chen et al (eds) *Landslides and engineered slopes*. Taylor and Francis Group, London. ISBN:978-0-415-41196-7:1389-1395
- Bozzano F, Lenti L, Martino S, Paciello A, Scarascia Mugnozza G (2008c) Self-excitation process due to local seismic amplification responsible for the 31st October 2002 reactivation of the Salcito landslide (Italy). *J Geophys Res* 113:B10312. doi:10.1029/2007JB005309
- Caserta A, Ruggiero V, Lanucara P (2002) Numerical modelling of dynamical interaction between seismic radiation and near surface geological structures: a parallel approach. *Comput Geosci* 28(9):1069–1077
- Castello B, Selvaggi G, Chiarabba C, Amato A (2006) CSI Catalogo della sismicità italiana 1981-2002, version 1.1. INGV-CNT, Rome. Available at <http://www.ingv.it/CSI/>
- CFTI3 (2000) Catalogue of strong Italian earthquakes from 461 a.C. to 1997. ING-SGA, Bologna
- Chavez-Garcia FJ, Sanchez LR, Hatzfeld D (1996) Topographic site effects and HVSR. A comparison between observation and theory. *Bull Soc Seismol Am* 86:1559–1573
- CPTI04 (2004) Catalogo Parametrico dei Terremoti Italiani dal 217 a.C. al 2002. INGV. website: <http://emidius.mi.ingv.it/CPTI04/>
- Cruden DM, Varnes DJ (1996) Landslide types and processes. In: Turner AK, Schuster RL, (eds) *Landslides: investigation and mitigation*. Transportation Research Board, Spec. Report 247. National Research Council, National Academy Press, Washington, DC, pp 36–75
- DBMI04 (2004) Database Macrosismico Italiano. INGV site: <http://emidius.mi.ingv.it/DBMI04>
- Del Gaudio V, Wasowski J (2007) Directivity of slope dynamic response to seismic shaking. *Geophys Res Lett* 34:L12301. doi:10.1029/2007GL029842
- Dipartimento della Protezione Civile (2004) The strong motion records of Molise sequence (October 2002–December 2003). Ufficio Servizio Sismico Nazionale, Servizio Sistemi di Monitoraggio, Rome (CD-ROM)
- Faccioli E (1995) Induced hazard: earthquake triggered landslides. In: *Fifth international conference on seismic zonation*, Nice. 3:1908–1931
- Field EH, Jacob K (1995) A comparison and test of various site response estimation techniques, including three that are non reference-site dependent. *Bull Seismol Soc Am* 85:1127–1143
- Fukuoka H, Sassa K, Scarascia Mugnozza G (1997) Distribution of landslides triggered by the 1995 Hyogo-Ken Nanbu earthquake. *J Phys Earth* 45:83–90
- Gallipoli M, Lapenna V, Lorenzo P, Mucciarelli M, Perrone A, Piscitelli S, Sdao F (2000) Comparison of geological and geophysical prospecting techniques in the study of a landslide in southern Italy. *Eur J Environ Eng Geophys* 4:117–128
- Giunta G, Luzio D, Tondi E, De Luca L, Giorgianni A, D'Anna G, Renda P, Cello G, Nigro F, Vitale M (2004) The Palermo (Sicily) seismic cluster of September 2002, in the seismotectonic framework of the Tyrrhenian Sea–Sicily border area. *Ann Geophys* 47:1755–1770
- Gruppo di Lavoro (2004) Redazione della Mappa di Pericolosità Sismica prevista dall'Ordinanza del 20/03/2003 n. 3274 All. 1, per il Dipartimento di Protezione Civile, INGV, Milano-Roma, April 2004, p 65 + 5 annexes

- Havenith HB, Jongmans D, Faccioli E, Abdrakhmatov K, Bard PY (2002) Site effect analysis around the seismically induced Anavevo rockslide, Kyrgyzstan. *Bull Seismol Soc Am* 92(8):3190–3209
- Havenith HB, Strom A, Jongmans D, Abdrakhmatov K, Delvaux D, Tréfois P (2003a) Seismic triggering of landslides, part A: field evidence from the northern Tien Shan. *Nat Hazards Earth Syst Sci* 3:135–149
- Havenith HB, Vanini M, Jongmans D, Faccioli E (2003b) Initiation of earthquake-induced slope failure: influence of topographical and other site specific amplification effects. *J Seismol* 7:397–412
- Hutchinson JN (1987) Mechanism producing large displacements in landslides on pre-existing shears. *Mem Soc Geol China* 9:175–200
- Hutchinson JN (1988) General report: morphological and geotechnical parameters of landslides in relation to geology and hydrogeology. In: *Proc 5th Int Symp on Landslides, Lausanne*. Balkema, Rotterdam, pp 3–36
- INGV (2006) Mappa di pericolosità sismica del territorio nazionale. Available at [http://zonesismiche.mi.ingv.it/mappa\\_ps\\_apr04/italia.html](http://zonesismiche.mi.ingv.it/mappa_ps_apr04/italia.html)
- ITASCA (2005) FLAC 5.0: user manual. Licence number 213-039-0127-16143, Earth Science Department, Sapienza–University of Rome
- Jibson RW (1993) Predicting earthquake-induced landslide displacements using Newmark's sliding block analysis. In: *Transportation research record 1411*, TRB, National Research Council, Washington DC, pp 9–17
- Keefer DK (1984) Landslides caused by earthquakes. *Geol Soc Am Bull* 95:406–421
- Kuhlemeyer RL, Lysmer J (1973) Finite element method accuracy for wave propagation problems. *J Soil Mech Found Div ASCE* 99(SM5):421–427
- Lenti L and Martino S (2009) New procedure for deriving multifrequency dynamic equivalent signals: numerical implementation and case study based on Italian accelerometric records. *Bull Earthq Eng*. doi:10.1007/s10518-009-9169-7
- Lenti L, Martino S, Paciello A, Scarascia Mugnozza G (2009) Evidences of 2D amplification effects in an alluvial valley (Valnerina, Italy) from velocimetric records and numerical models. *Bull Seismol Soc Am* 99(3):1612–1635. doi:10.175/0120080219
- Lin ML, Wang KL and Kao TC (2008) The effects of earthquake on landslides. A case study of Chi-Chi earthquake, 1999. In: Chen et al (eds) *Landslides and engineered slopes*. Taylor and Francis Group, London, pp 193–201. ISBN:978-0-415-41196-7
- Liu HP, Anderson DL, Kanamori H (1976) Velocity dispersion due to anelasticity: implications for seismology and mantle composition. *Geophys J R Astron Soc* 47:41–58
- Luzi L, Pergalani F (1996) Application of statistical and GIS techniques to slope instability zonation (1:50,000 Fabriano geological map sheet). *Soil Dyn Earthq Eng* 15:83–94
- Luzi L, Pergalani F (2000) A correlation between slope failures and accelerometric parameters: the 26th September 1997 earthquake (Umbria-Marche, Italy). *Soil Dyn Earthq Eng* 20:301–313
- Mahdaviifar M, Jafari MK, Zolfaghari MR (2008) GIS-based real time prediction of Arias intensity and earthquake-induced landslide hazards in Alborz and Central Iran. In: Chen et al (eds) *Landslides and engineered slopes*. Taylor and Francis Group, London. ISBN:978-0-415-41196-7:1427–1438
- Martino S, Scarascia Mugnozza G (2005) The role of the seismic trigger in the Calitri landslide (Italy): historical reconstruction and dynamic analysis. *Soil Dyn Earthq Eng* 25:933–950
- Martino S, Paciello A, Sadoyan T, Scarascia Mugnozza G (2007) Dynamic numerical analysis of the giant Vokhchaberd landslide (Armenia). In: *Proc 4th international conference on earthquake geotechnical engineering, Thessaloniki, Greece, 25–28 June 2007*, Paper no. 1735
- Méric O, Garambois S, Jongmans D, Wathélet M, Chatelain JL, Vengeon JM (2005) Application of geophysical methods for the investigation of the large gravitational mass movement of Séchillienne. *Fr Can Geotech J* 42:1105–1115
- Méric O, Garambois S, Malet JP, Cadet H, Guéguen P, Jongmans D (2007) Seismic noise-based methods for soft-rock landslide characterization. *Bull Soc Géol Fr* 178(2):137–148
- Miles SB, Ho CL (1999) Rigorous landslide hazard zonation using Newmark's method and stochastic ground motion simulation. *Soil Dyn Earthq Eng* 18(4):305–323
- Mozco P, Bard PY (1993) Wave diffraction, amplification and differential motion near strong lateral discontinuities. *Bull Seismol Soc of Am* 83(1):85–106
- Nakamura Y (1989) A method for dynamic characteristics estimation of subsurface using microtremor on the ground surface. *Q Rep RTRI* 30(1):25–33
- Newmark NM (1965) Effects of earthquakes on dams and embankments. *Geotechnique* 15:139–159
- Prestininzi A, Romeo R (2000) Earthquake-induced ground failures in Italy. *Soil Dyn Earthq Eng* 58:387–397
- Rodriguez CE, Bommer JJ, Chandler RJ (1999) Earthquake-induced landslides: 1980–1997. *Soil Dyn Earthq Eng* 18:325–346
- Romeo R (2000) Seismically induced landslide displacements: a predictive model. *Eng Geol* 58(3/4):337–351
- Roten D, Cornou C, Steimen S, Fäh D, Giardini D (2004) 2D resonances in Alpine valleys identified from ambient vibration wavefield. In: *Proc 13th World Conf Earth Eng, Vancouver, Canada*. IAEE, Tokyo, paper 1787, p 6
- Santoni D, Giuffrida C, Ruggiero V, Caserta A, Lanucara P (2004) Web user-friendly interface to produce input data for numerical simulations of seismic wave propagation problem. *Geophys Res Abstr* 6:06020
- Sassa K (1996) Prediction of earthquake induced landslides. Senneset K (ed) *Landslides*. Balkema, Rotterdam, pp 115–132
- Sassa K, Fukuoka H, Scarascia Mugnozza G, Evans S (1996) Earthquake induced landslides: distribution, motion and mechanisms. *Soils and Foundations Special Issue*, pp 53–64
- Sassa K, Fukuoka H, Wang F, Wang G (2005) Dynamic properties of earthquake-induced large-scale rapid landslides within past landslide masses. *Landslides* 2:125–134
- Seed HB (1979) Soil liquefaction and cyclic mobility evaluation for level ground during earthquakes. *J Geotech Eng Div ASCE* 105(GT2):102–155
- Seed HB, Idriss IM (1969) Influence of soil conditions on ground motion during earthquakes. *J Soil Mech Found Div ASCE* 1969(95):99–137
- Sieberg A (1930) Mercalli-Cancani-Sieberg (MCS) macroseismic scale. *Geologie der Erdbeben, Handbuch der Geophysic*, Berlin, pp 552–555
- Spudich P, Hellweg M, Lee WHK (1996) Directional topographic site response at Tarzana, observed in aftershocks of the 1994 Northridge, California, earthquake: implications for main shock motions. *Bull Seismol Soc Am* 86:S193–S208
- Steimen S, Fäh D, Kind F, Schmid C, Giardini D (2003) Identifying 2-D resonance in microtremor wave fields. *Bull Seismol Soc Am* 93:583–599
- Tika TE, Vaughan PR, Lemos LJ (2008) Fast shearing of pre-existing shear zones in soils. *Geotechnique* 46(2):197–233
- Tiwari B, Dhungana I, Garcia CF (2008) Reduction of the stability of pre-existing landslides during earthquakes. In: Chen et al (eds)

- Landslides and engineered slopes. Taylor and Francis Group, London, pp 1463–1467. ISBN:978-0-415-41196-7
- Towhata I, Shimomura T, Mizuhashi M (2008) Effects of earthquakes on slopes. In: Chen et al. (eds) Landslides and engineered slopes. Taylor and Francis Group, London, pp 53–65. ISBN:978-0-415-41196-7
- Zienkiewicz OP (2005) The finite element method. McGraw–Hill, London, p 785